UNIVERSITY OF COPENHAGEN
FACULTY OF SCIENCE
„,

PhD thesis

Michael. J. Larson

A Search for Tau Neutrino Appearance with IceCube-De

Advisor: Dr. D. Jason Koskinen

Handed in: March 7, 2018

Contents

List of Figures

List of Tables

Introduction

1

Measurements of atmospheric neutrino oscillations, such as those performed in this thesis, require a background of understanding of both atmospheric neutrinos as well as neutrino oscillations. A history of neutrinos (Section 1) is used to explain the discovery of the three known flavors of neutrinos as well as the difficulties inherent in the study of these elusive particles. A discussion of the history of cosmic rays (Section 1.1) explains the source of both the neutrinos (Section 1.2) used as signal in this thesis as well as the muons, which form one of the primary backgrounds in the search for atmospheric oscillations.
The detection of neutrinos is described in two parts. A discussion of the neutrino interactions (Section 1.4), explains the interactions of neutrinos with matter. The detection of these interactions through electromagnetic emission is then covered (Section 1.4.1).

1.1 The History of the Neutrino

In 1896, Henri Becquerel discovered radioactivity in uranium [1]. Measurements over the following decades showed various types of nuclear decays based on the penetration depth of the ionizing emissions. Measurements of one type of radioactivity, the beta decays, over the following 30 years showed that the production of two observed particles from one parent nucleus: a daughter nucleus and an outgoing electron. A single body decay of this type produces a known spectrum due to conservation of energy and momentum. The energy of the daughter nucleus and the electron are completely determined by these two conditions, leading to a narrow line emission spectrum.
Contrary to expectations, however, the measurement of energies of the two resulting particles showed wide, continuous spectra [2]. The spectrum provided a major puzzle for physicists due to the contradition with the simple theoretical expectations. A conundrum for many years, one possible solution was suggested in 1930 by Wolfgang Pauli. In his letter, Pauli suggested that the conservation of energy and momentum could be saved if "... there could exist in the nuclei electrically neutral particles... which have spin 1/2 and obey the exclusion principle, and additionally different from light quanta in that they do not travel with the velocity of light" [3]. The solution to the beta decay puzzle was, then, that this additional "neutron" particle was emitted simultaneously with the observed daughter particles. This newly proposed particle would be electrically neutral and, therefore, unable to be seen through traditional methods. The resulting spectrum of the observed particles could then be continuous, as verified experimentally.
Pauli's suggestion provided a way to save the beloved conservation laws in physics, but at the expense of the assumption of a new particle. The particle, called the "neutron" in Pauli's letter and later renamed the "neutrino" by Fermi, was proposed to be electrically neutral and, therefore, completely undetectable at the time. Later work proposed that the neutrinos interact only via the weak nuclear force, with an interaction strength many orders of magnitude smaller than electromagnetic and strong nuclear forces. Experimental measurements, sensitive only to electromagnetic forces, therefore cannot be used to study neutrinos directly in the same way that other particles may be measured.
It was not until nearly 20 years later, in 1956, that this mystery particle was first detected [4]. In a groundbreaking work, Cowen and Reines presented an experiment at the Savannah River Plant, a nuclear power plant, demonstrating detection of the neutrino. The experiment, made up of layers of scintillation detectors around polyethelene boxes,

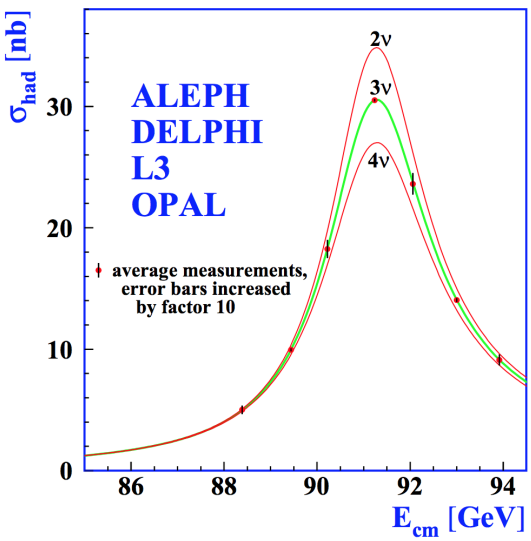

Figure 1.1 – The number of active neutrinos as measured by ALEPH, DELPHI, L3, and OPAL. The data from the four experiments strongly favors only three neutrinos coupling to the Z boson. Image taken from [9].

yielded a signal-to-background rate of about 3 to 1 with a rate of 2.88 ± 0.22 counts/hour with a total livetime of 1371 hours, including time during which the nearby nuclear reator was offline. For the discovery of the first neutrinos, Frederick Reines was granted a shared Nobel Prize in Physics for the year 1995 [5].

Since the neutrino was first observed, additional measurements have discovered two new flavors of neutrinos: the muon neutrino [6] and the tau neutrino [7, 8].

Searches for additional neutrinos beyond the discovered three have been performed by investigating the decays of the Z boson. The Z boson, a particle of 91 GeV [**pdg**], couples both to the neutrinos and to more easily observed hadrons and charged leptons making it a useful probe of neutrino interactions. The width of the Z decay to hadrons, for instance, is affected by the number of active, light neutrino species [9]. Additional flavors of neutrinos coupling to the Z boson would lead to a smaller decay rate to hadrons observed in accelerator searches for hadrons as shown in Figure **??**. The number of neutrinos may be calculated by comparing the best-fit ratio of "invisible" decays of the Z boson (ie, those involving two neutrinos) to the measured width expected from charged leptons in the standard model.

$$R_{inv} \equiv \frac{\Gamma_{inv}}{\Gamma_{ll}} = N_\nu \left(\frac{\Gamma_{\nu\nu}}{\Gamma_{ll}}\right)_{SM} \tag{1.1}$$

Here the number of neutrinos is extracted by assuming that all active neutrinos have the same coupling to the Z boson, result which has been verified experimentally. A precision measurement of the Z resonance completed at the LEP coillider found the best fit value of $N_\nu = 2.9840 \pm 0.0082$, in good agreement with only three active neutrinos.

1.2 History of Cosmic Rays

In the early years of the 20th century, scientists began investigating previously-unknown ionizing radiation in the atmosphere. Scientists using electroscopes, early instruments designed to measure electric charge and radiation, discovered low levels of radiation

in the air. This new radiation was observed to be reduced when the electroscope was shielded by metal free of radioactivity, indicating that the signal was not an artifact of the detector itself and was, instead, coming from an external source.
Following just a few decades after the discovery of radioactivity by Becquerel, many scientists believed that the electroscope was picking up radiation from the Earth itself. The rate would be expected to decrease with increasing altitude above sea level and, to increase with increasing depth in the sea. Early measurements by Domenico Pacini in 1910 showed that the radiation rate decreased by 20% at a depth of 3 meters underwater compared to the rate at the surface [10], implying an origin independent of the Earth's crust. Measurements were performed with electroscopes by Victor Franz Hess in 1912 of the rate of ionizing radiation up to an altitude of 5 km [11].
Hess showed that the observed rate decreased until an altitude of around 1 km, but at a slower rate than expected from theory. Above 1400 meters, however, the rate of ionizing radiation increased again, rising substantially up to the maximum altitude reached at 5300 meters [12]. Hess's work, later confirmed by Henri Millikin, showed definitively that there exists a source of radiation of extraterrestrial origin, earning him the Nobel Prize in Physics for 1936 [13]. This radiation was later dubbed "cosmic rays" by Millikan in reference to their extraterrestrial origin.
Work on cosmic rays has lead to numerous discoveries. In 1937, the first *hadronic showers* were observed [14]. Hadronic showers of particles created by interactions of cosmic rays were shown to produce large numbers of particles [15, 11], with many producing from 5×10^6 to over 10^9 particles [16]. These showers begin with a cosmic ray primary particle, often a single proton accelerated to high energies, which interacts with particles of the Earth's atmosphere. The interaction leads to the creation of various daughters, including neutrinos, muons, pions, kaons, and other hadrons.
Modern measurements have shown that the cosmic ray spectrum primarily consists of protons with a small contribution from helium and heavier elements [17] These ions are accelerated in unknown astrophysical sources up to extremely high energies. The cosmic ray spectrum extends over many orders of magnitude, with the highest energy observations reaching 10^{20} electronvolts - far higher than any Earth-based accelerator. The spectrum, shown in Figure 1.2, has multiple features that are believed to arise from different accelerator sources at different scales, each of which has been verified by multiple experiments.

1.3 Atmospheric Neutrinos

Air showers from cosmic rays provide a useful natural source of neutrinos in the GeV energy range and above that may be used for fundamental physics research. The hadronic shower produces pions and kaons which, in turn, decay to produce neutrinos

$$\pi^+ \rightarrow \mu^+ \nu_\mu \rightarrow e^+ \nu_e \bar{\nu_\mu} \nu_\mu \tag{1.2}$$

from the pions and from the kaons

$$K^+ \rightarrow \pi^+ \nu_\mu \rightarrow e^+ \nu_e \bar{\nu_\mu} \nu_\mu \nu_\mu \tag{1.3}$$

The neutrino flux depends on a number of parameters, including the Earth's magnetic field and temperature profile, the cosmic ray flux, and the details of hadronic interactions in air showers [18]. The calculation of the neutrino flux predictions requires significant, dedicated simulation work, producing fluxes as both a function of energy (Figure 1.3) and direction (Figure 1.4).

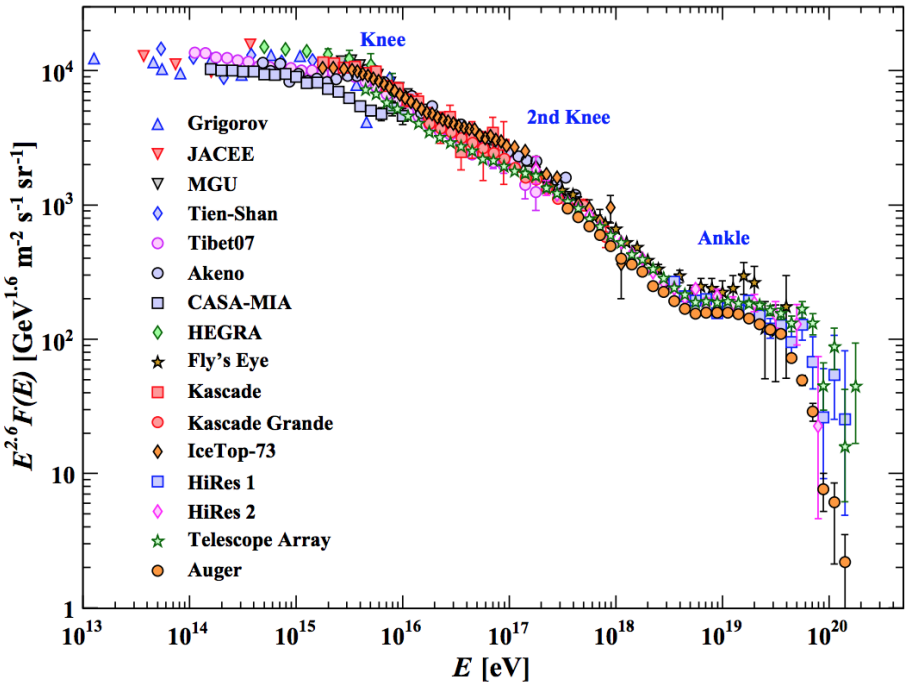

Figure 1.2 – The cosmic ray spectrum covers many orders of magnitude and has been verified by many experiments to high precision. The various features are thought to be caused by multiple sources at different scales. Image taken from [17]

1.4 The Standard Model

Muons and neutrinos form just a small part of the Standard Model of particle physics. The Standard Model, with fundamental particle types and properties shown in Figure 1.5, consists of six quarks (up, down, strange, charm bottom, and top), three charged leptons (electron, muon, tau), three uncharged leptons (electron neutrino, muon neutrino, and tau neutrino), and the five bosons related to interactions (photon, Z, W, gluon, and Higgs). Combinations of the quarks lead to various hadrons, paticles which interact with and are formed via the strong force, with different combinations of quarks and anti-quarks producing a wide variety of particles. The Standard Model, developed over the last half century, elegantly encapulates the range of phenomena known to occur in particle physics and has been verified repeatedly over decades by many experiments. Predictions of the Standard Model have been carefully verified by accelerator experiments, yielding precise checks on a wide range of parameters.

The three charged leptons and neutrinos form three "families" or "flavors". Each charged lepton posseses a coupled neutrino which shares a lepton number conserved in interactions. The electron, the lightest of the charged leptons at 511 keV [17], is a key ingredient of the atoms that make up the world, forming the basis for all of chemistry and is the only stable charged lepton. The muon, with a mass of 105.7 MeV, is the middle of the three charged leptons, often appearing in particle interactions accompanied by the muon neutrino. The muon has a relatively long livetime of 2.197 microseconds, far longer than many unstable hadrons. The tau lepton is the heavies of the leptons, and with a mass of 1.777 GeV, it is heavier than the proton and appears only in relatively high energy interactions. The tau has an extremely short lifetime, at 290.6 femtoseconds, and a rich

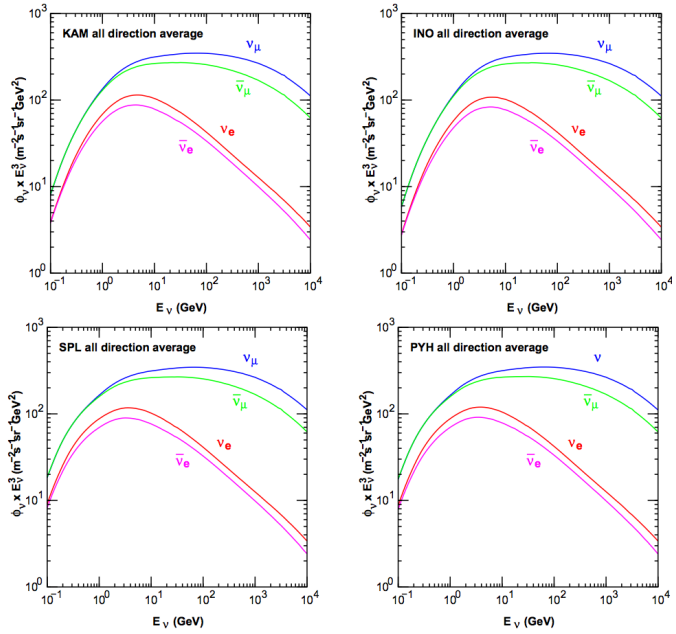

Figure 1.3 – The expected neutrino flux at Kamioka mine, Japan (Super-Kamiokande, top left), Ino Peak, India (India-based Neutrino Observator, top right), the South Pole (IceCube, bottom left), and Pyhasalmi mine, Finland (EMMA experiment, bottom right) as a function of energy. Note that the neutrino and anti-neutrino fluxes are characterized separately. The differences in the flux at each site is due to differences in the Earth's magnetic field and temperature profile. Figure taken from [18].

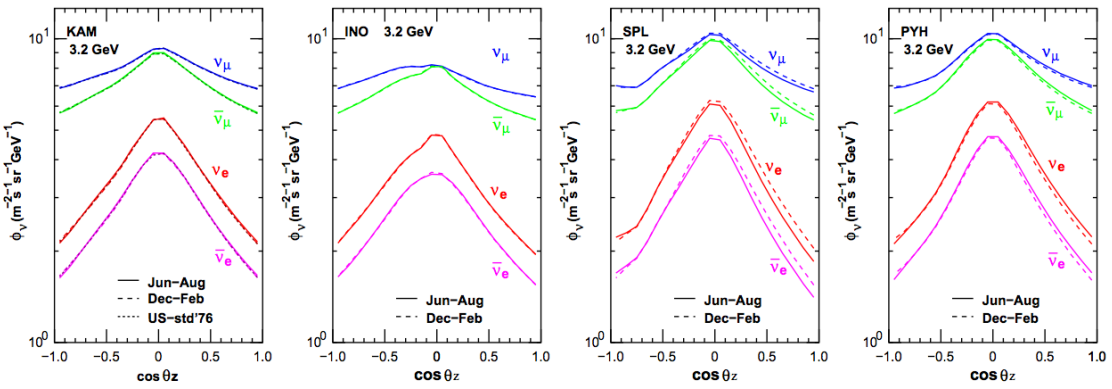

Figure 1.4 – The expected flux of 3.2 GeV neutrinos at Kamioka mine, Japan; Ino Peak, India; the South Pole; and Pyhasalmi mine, Finland as a function of zenith angle. A value of $\cos\theta_Z = -1$ indicates neutrinos passing through the entire Earth and entering the detector from below while a value of $\cos\theta_Z = +1$ indicates neutrinos interacting in the atmosphere directly above the detector. The differences in the flux at each site is due to differences in the Earth's magnetic field and temperature profile. Figure taken from [18].

variety of decay products. This extremely short lifetime and high mass make the tau difficult to produce and study.

For the purposes of this work, the most significant parts of the Standard model are the neutrinos, which will be defined to be signal events; the up and down quarks, which will make up the protons and neutrinos upon which the neutrinos will interact; the W and Z

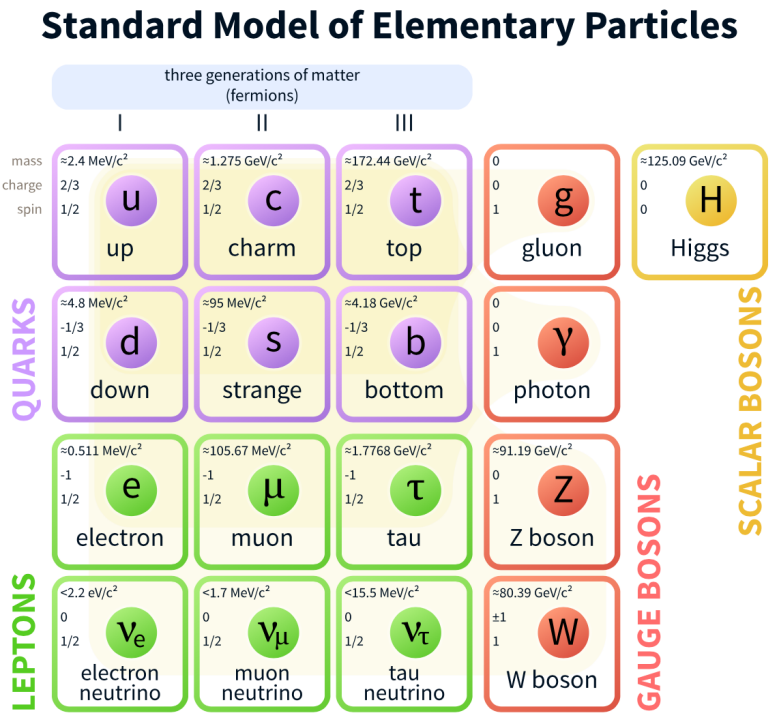

Figure 1.5 – The Standard Model of particle physics is made up of charged and uncharged leptons, quarks, and the various bosons. Image taken from [19]

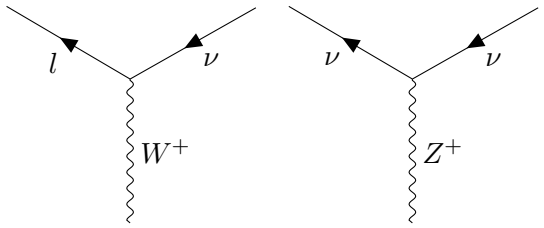

Figure 1.6 – Feynman diagrams showing the interaction vertex of the neutrino with the W and Z boson.

bosons, which mediate the weak interactions via which the neutrinos may be observed; and the photon, which gives a method of observation of the interactions.

1.4.1 Neutrino Interactions

In the Standard Model, neutrinos are assumed to be massless, left-handed spin-1/2 leptons which interact solely via the weak force. Neutrinos, therefore, are only visible via indirect effects, such as scattering or production of charged particles that may, in turn, give off their own visible signature. An understanding of the methods by which neutrinos are detected therefore forms an important basis for the study of these elusive particles. Two basic Feynman diagrams, shown in Figure 1.6, may be used to represent the interaction verticies available for neutrinos.

These two vertices describe the interactions relevent for the work presented in this thesis. During so-called *charged-current* (CC) interactions, a $\mathtt{W}^{\pm}$ boson is exchanged between a neutrino and target particle, in the process converting the uncharged neutrino to the corresponding charged lepton. The *neutral-current* (NC) interactions are those in which

the uncharged Z boson is exchanged with the target and the neutrino, although losing a fraction of the initial energy, does not get converted to a charged lepton.
Detectors used to study particle properties rely on electromagnetic interactions and photons in order to detect particles. Because the neutrino itself does not interact via the electromagnetic force, charged leptons and hadrons must be used to indirectly study the properties of the incident neutrinos. Outgoing charged leptons in charged-current interactions may be detected, although the direction will not necessarily correspond to that of the incident neutrino. The average angle between the incident neutrino and outgoing lepton may be approximated following Equation 1.4.

$$\bar{\theta}_{\nu l} \approx \frac{1.5°}{\sqrt{E_\nu\,[TeV]}} \tag{1.4}$$

There exist three further classifications of neutral-current and charged-current neutrino interactions in the energy range used in this work: the quasi-elastic, resonant, and deep inelastic interactions [20]. A fourth type, coherent neutrino scattering, may also occur, although the energies involved are too low to impact this work. The three types of interactions are contribute to the total cross-section with peaks at different energies, as shown in Figure 1.7.

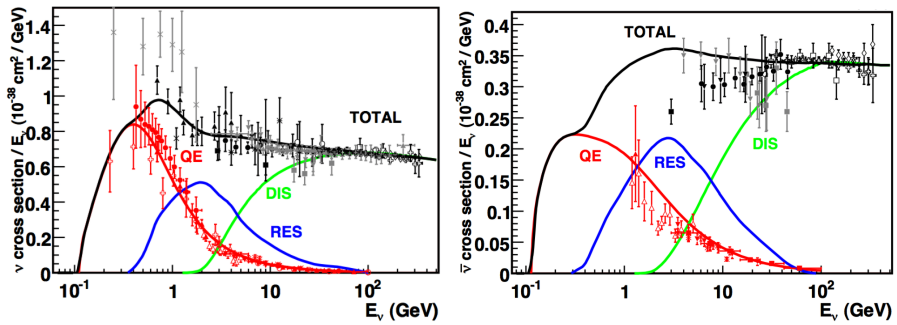

(a) ν Interaction Cross-sections **(b)** $\bar{\nu}$ Interaction Cross-sections

Figure 1.7 – The relative contributions to the cross section for ν (left) and $\bar{\nu}$ (right). The QE events dominate below 1 GeV while the DIS events dominate above 10 GeV. Note the different scales for the neutrino and antineutrinos. Images taken from [20]

Quasi-Elastic and Resonant Interactions

At low energies of approximately 100 MeV to around 2 GeV, the neutrinos interact via *quasi-elastic scattering* (*QE*) interactions. In the QE interaction, the neutrino scatters off an entire nucleon instead of the individual quarks. In a charged current QE neutrino (anti-neutrino) interaction, the target neutron (proton) is converted to a proton (neutron) while the neutrino is converted to a charged lepton.
The cross section for QE interactions depends on various nuclear form factors that must be fit to experimental data. Many of these form factors may be fit to electron scattering data, leaving only the axial vector nuclear form factors to be measured in the neutrino sector [20]. This form factor is normally assumed to have the dipole form

$$F_A\left(Q^2\right) = \frac{g_A}{\left(1 + \frac{Q^2}{M_A^2}\right)^2} \tag{1.5}$$

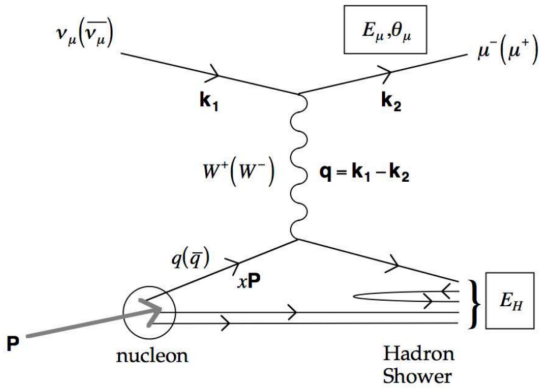

Figure 1.8 – A Feynman diagram showing an example of a CC neutrino DIS interaction. An incident muon neutrino interacts with a quark inside of a proton. The result is a hadronic shower as well as a charged muon. Diagram taken from [**formaggio-xsec**]

where g_A is a constant fit to experimental data, Q^2 is the 4-momentum transferred in the interaction, and M_A is the "axial mass". This last term is fit to experimental data with a value of $M_A = 0.999 \pm 0.011$ GeV [20].
Resonant scattering interactions (*RES*), which result in the excitation of a nucleon followed by decay via emission of (typically) pions, occur for neutrinos of slightly higher energies of around 500 MeV to 10 GeV. Resonant interactions are modeled in a similar way as the quasi-elastic interactions, with an associated axial mass term used to describe nuclear uncertainties.

Deep Inelastic Interactions

Above a few GeV, the neutrino cross section rises approximatley linearly with energy and is dominated by *deep inelastic scattering* (*DIS*) interactions. An example of a DIS interaction is shown in Figure 1.8. In DIS events, the exchange of the Z or W boson probes the internal structure of the nucleons, leading to a scattering off of the individual quarks of the nucleus. This results in disruption of the nucleon and the larger nucleus and a collection of daughter particles forming a *hadronic shower*.
As seen in Figure 1.7, the DIS events dominate the neutrino cross section above 10 GeV and form the only significant interaction above 100 GeV [**formaggion-xsec**]. Experiments with high statistics samples of DIS events have been used to measure the charged current cross section to the few-percent level.

1.5 Methods of Detection

Neutrinos may be detected through the QE, RES, and DIS interaction channels, with each possessing a distinct signature. The interaction of neutrinos at the GeV energy ranges relevent for this thesis lead to the emission of hadrons in a hadronic shower. The lower energy QE and RES interactions typically yield only one pion which may decay into a pair of photons (π^0) or into further charged hadrons and leptons ($\pi^\pm$). DIS interactions produce larger hadronic showers containing many charged particles that may be detected. In addition to the hadronic shower, charged-current interactions result in an outgoing charged lepton, the result of which depends on the flavor of the incident neutrino. Outgoing electrons quickly scatter in interactions with the surrounding media, ionizing atoms and producing a secondary *electromagnetic shower* of particles. Muons, on the

Decay	Branching Ratio	Background
$\tau \to e^{-}\nu_e\nu_\tau$	17.83 ± 0.04 %	ν_e CC
$\tau \to \mu^{-}\nu_\mu\nu_\tau$	17.41 ± 0.04 %	ν_μ CC
$\tau \to$ hadrons	Otherwise	ν NC

Table 1.1 – The branching ratios for the decay of tau leptons. Two-thirds of the time, the tau lepton decays hadronically.

other hand, travel longer distances before scattering or decaying in the medium, leading to an extended track.

The signature of a tau neutrino charged current interaction varies depending on the specific decay channel of those presented in 1.1. Because the tau lepton has a very short lifetime, outgoing taus tend to decay immediately, producing daughter particles. Each of the three decay modes mimic interactions of the electron and muon neutrinos. The secondary electromagnetic or hadronic cascade is theoretically distinguishable from the primary hadronic cascade produced by a tau neutrino charged current interaction, although the distance traveled by the tau lepton at the energies relevent for this work is on the order of millimeters, far below the reconstruction precision possible with the IceCube detector.

In each case, the charged particles deposit energy into the interaction medium during travel through a series of stochastic and continuous emissions. It is through the detection of these stochastic and continuous losses that daughter particles may be identified in the study of neutrinos.

1.5.1 Stochastic Emission Mechanisms

A total of five major stochastic emission mechanisms are important for the energy losses in neutrino experiments [21]. One such mechanism is the decay of the particle, a process which splits the energy of the parent into multiple, lower energy daughters. Decays of daughter leptons can often by important in the identification of the neutrino flavor, particularly for tau neutrino candidates occuring above 10 TeV when the primary and secondary hadronic interactions become well-separated.

Ionization losses occur when the charged lepton interacts with electrons in the medium, transferring enough energy to librerate the electrons from bound states. At energies below 1 TeV, these losses are the most significant form of energy loss for charged particles, producing a significant source of additional electrons. Ionization losses occur roughly independently of the energy of the charged lepton.

Above energies of a few hundred GeV, radiative processes dominate the energy losses for muons in matter [17]. Bremmstrahlung, photon emission from charged particles accelerating in a magnetic field, pair production, in which a particle and antiparticle (typically electron and positron) are created, and hadronic interactions of photons all dominate the energy losses of muons above 1 TeV.

There exists a minimum in the energy loss rates. Particles emitting near this minimum rate are known as *minimum-ionizing* particles [17].

Stochastic emissions result in additional particles in the detector, leading to improved light yield. In addition, some detectors use photosensitive emulsions [22, 7], scintillators [23, 24, 25, 26], or time projection chambers [27] in order to track ionization losses. These emulsions yield precise characterization of particle decays, allowing experimentalists to uniquely determine the flavor state of the interacting neutrino.

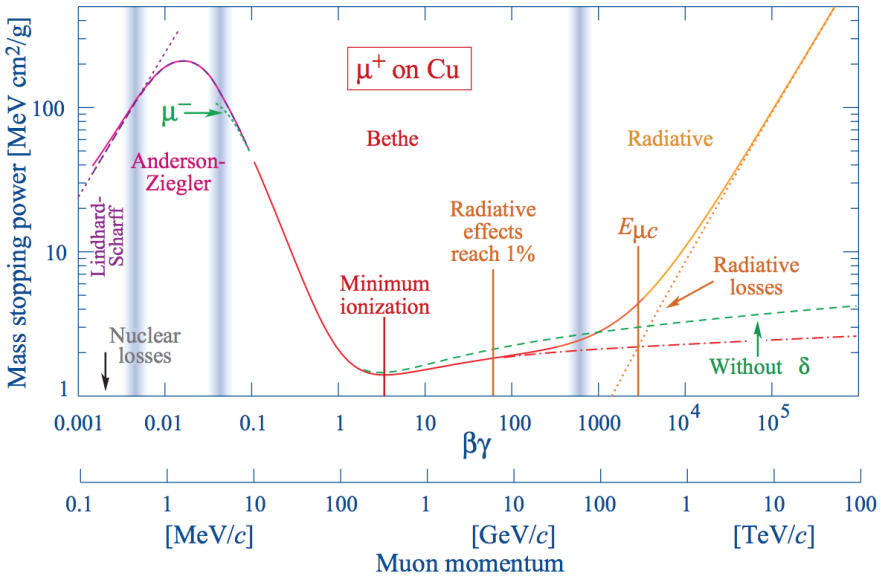

Figure 1.9 – An example of the energy loss ($\frac{-dE}{dX}$) calculated for muons incident on copper. Note the radiative losses due to bremsstrahlung, pair production, and photonuclear interactions above 1 TeV. Note also the labeled minimum demonstrating the energy of a minimum ionizing particle. Image taken from [17].

1.5.2 Cherenkov Emission

When a charged particle passes through a dielectric medium with a speed larger than the local phase velocity of light, it will emit *Cherenkov radiation*[28]. The effect, first reported by Pavel Cherenkov in 1934 [29] remained unexplained theortically until work done by Ilya Frank and Igor Tamm in 1937 [30].

For a dielectric medium, the electric field of the charged particle will polarize atoms by inducing a small dipole moment due to electromagetic effects in nuclei of atoms in the medium [31]. The resulting disturbance of the medium propagates with the phase velocity of light, given by the speed of light, c, and the index of refraction as a function of the frequency of light, $n(\omega)$. If the charged particle is traveling faster than the local phase velocity, the electromagnetic disturbance propagates with constructive interference, resulting in a planar wavefront of emission known as *Cherenkov emission*. The angle of the wavefront relative to the propagation direction is given by the ratio of the distance traveled by the particle and photons in a given time.

$$cos(\theta_C) = \frac{\frac{c}{n(\omega)}t}{vt} = \frac{c}{n(\omega)v}, \tag{1.6}$$

The energy threshold for Cherenkov emission is set by a combination of the particle mass and the local phase velocity for light, $\frac{c}{n}$. Using the relativitistic kinetic energy [32],

$$E_C \geq \frac{mc^2}{\sqrt{1-\left(\frac{c/n}{c}\right)^2}} \tag{1.7}$$

$$E_C \geq mc^2\sqrt{\frac{n^2}{n^2-1}} \tag{1.8}$$

For ice with a index of fraction of 1.32 at 400 nanometers [33], this works out to a minimum energy of 270 keV for electrons and 56.2 MeV for muons. The number of photons emitted increases with energy, with approximately 50% more photos produced in blue visible light than in red[32] The full emission spectrum, first worked out by Ilya Frank and Igor Tamm in 1937 [30], depends on a number of parameters, including the energy and charge of the emitting particle as well as the properties of the medium. In the case of a particle traveling a distance L much larger than the photon frequency of interest, λ, the number of emitted photons may be approximated by

$$\frac{dN}{d\lambda} = \frac{2\pi\alpha}{\lambda^2} L sin^2\theta_C \quad L >> \lambda \tag{1.9}$$

Cherenkov emission is not limited to a single charged lepton. All charged particles emit Cherenkov radiation, including any hadrons and charged daughter particles, resulting in measurable signals. While the total amount of energy lost via Cherenkov emission is small relative to losses due to stochastic processes, this emission type is both continous and results directly in photons which may be observed by photodetectors. This technique is used by multiple experiments, including SNO [34], Super-Kamiokande [35], ANTARES [36], and IceCube [37].

Neutrino Oscillations

2

The search for oscillation events requires an explanation of neutrino oscillations. The theory of neutrino oscillations is included here with broad descriptions of oscillations in vacuum (Section 2.1.1) and in matter (Section 2.1.2). Experimental evidence for the neutrino oscillations and current constraints on the oscillation parameters is presented in Section 2.1.3. Finally, a description of unitarity in the PMNS mixing matrix is given in Section 2.4.1 with particular emphasis placed on the search for additional neutrino flavors (Section 2.5). The motivation for this thesis as well as the purpose behind joint fits between appearance and disappearance data is discussed in Section 2.5.2.

2.1 Oscillation Theory and the PMNS Matrix

In 1968, Bruno Pontecorvo suggested a process, known as *neutrino oscillation*, by which neutrinos could change flavors [38]. The theory of neutrino oscillations was further developed for the neutrino sector by Ziro Maki, Masami Nakagawa and Shoichi Sakata in 1962 [39].

2.1.1 The PMNS Mixing Matrix

We now understand there to be three distinct flavors of neutrinos. Neutrinos are created via the weak force as pure flavor eigenstates. These states are coherent superpositions of mass eigenstates. Specifically, there exist three weak eigenstates of the left-handed neutrino fields that are related to three known neutrino mass eigenstates via the Pontecorvo-Maki-Nakagawa-Sakata (*PMNS*) lepton mixing matrix.

$$\begin{pmatrix} \nu_e \\ \nu_\mu \\ \nu_\tau \end{pmatrix} = U_{PMNS} \begin{pmatrix} \nu_e \\ \nu_\mu \\ \nu_\tau \end{pmatrix} = \begin{pmatrix} U_{e1} & U_{e2} & U_{e3} \\ U_{\mu 1} & U_{\mu 2} & U_{\mu 3} \\ U_{\tau 1} & U_{\tau 2} & U_{\tau 3} \end{pmatrix} \begin{pmatrix} \nu_1 \\ \nu_2 \\ \nu_3 \end{pmatrix} \tag{2.1}$$

The flavor eigenstates $(\nu_e, \nu_\mu, \nu_\tau)$ describe the fields of the left-handed neutrinos coupling via the weak charge to the electron, muon, and tau respectively. The three mass states (ν_1, ν_2, ν_3) represent the mass eigenstates. The mixing between the two types of states is given by the unitary matrix, U_{PMNS}. The mixing may be written in a shortened form

$$\nu_\alpha(x) = \sum_i U_{\alpha i} \nu_i(x) \tag{2.2}$$

where $\alpha = e, \mu, \tau$ and $i = 1, 2, 3$.

Neutrinos interact via the weak force and are created in flavor states e, μ, τ. The neutrino produced in flavor state ν_α exists in a superposition of the three mass eigenstates.

where δ_{ij} and $\delta_{\alpha\beta}$ are Kronecker delta functions. As a 3×3 unitary matrix, the PMNS matrix may be parametrized in terms of three mixing angles and six phases. Of these phases, five may be removed by rephasing the lepton fields with no change to the underlying physics, leaving one physical phase ralted to CP violation.

The PMNS may be written in terms of the product of three smaller unitary matrices using these mixing angles.

$$U_{PMNS} = \begin{pmatrix} 1 & 0 & 0 \\ 0 & c_{23} & s_{23} \\ 0 & -s_{23} & c_{23} \end{pmatrix} \begin{pmatrix} c_{13} & 0 & s_{13}e^{-i\delta_{CP}} \\ 0 & 1 & 0 \\ -s_{13}e^{i\delta_{CP}} & 0 & c_{13} \end{pmatrix} \begin{pmatrix} c_{12} & s_{12} & 0 \\ -s_{12} & c_{12} & 0 \\ 0 & 0 & 1 \end{pmatrix} \tag{2.3}$$

where the notation c_{ij} idenotes $\cos(\theta_{ij})$ and s_{ij} denotes for $\sin(\theta_{ij})$.
Note that if neutrinos are Majorana fermions, the additional phases may not be removed without making the masses complex. The Majorana terms form additional diagonal terms in Equation 2.3. While Majorana mass terms are beyond the scope of this work, further information may be found in [40, 41].
The three submatrices of Equation 2.3 have historically been studied by different types of experiments. This history has lead to the proliferation of alternative names for the matrices and of the mixing angles.

$$U_{PMNS} = U_{Atmospheric}U_{Reactor}U_{Solar} \tag{2.4}$$

This leads to the alternative names of the mixing angles, with θ_{23}, θ_{13}, and θ_{12} being referred to as the atmospheric mixing angle, the reactor mixing angle, and the solar mixing angle respectively.

2.1.2 Neutrino Mixing in Vacuum

Propagation of neutrinos requires the use of the Hamiltonian. However, the flavor states are not eigenstates of the Hamiltonian. For propagation of the neutrino, the mass eigenstates must instead be used.

$$|\nu(t=0)\rangle = |\nu_\alpha\rangle = \sum_i U^*_{\alpha i} |\nu_i\rangle \tag{2.5}$$

The propagation leads to a neutrino state at time $t \neq 0$ which is no longer a pure flavor state.

$$|\nu(t)\rangle = \sum_i U^*_{\alpha i} e^{-iE_i t} |\nu_i\rangle \tag{2.6}$$

where $E_i = \sqrt{p^2 + m_i^2}$ is the total energy of the ith mass eigenstate. If the neutrino state interacts, the flavor eigenstate must again be used to calculate the probabilities of interacting as each of the three known flavors.

$$P(\nu_\alpha \to \nu_\beta) = |\langle \nu_\beta | \nu(t) \rangle|^2 = \left| \sum_i U_{\beta i} U^*_{\alpha i} e^{-iE_i t} \right|^2 \tag{2.7}$$

Proper calculations from this point can be performed by treating each neturino as a quantum mechanical wave packet [42]. This allows for the full description of neutrino oscillation in the context of decoherence of the mass states during propagation, allowing each mass state to possess separate momenta.
In practice, the description of neutrino oscillations necessary for this work is adequately described by making a few simplifying assumptions. In particular, this work assumes that all mass eigenstates propagate as plane waves possessing identical, well-defined momenta [40]. Neutrinos are further assumed to be extremely relativistic at the energies of interest, an assumption well-justified by cosmological fits to the sum of the three

neutrino masses, which give an upper limit of around 0.2 eV [17]. The total neutrino energy is also assumed to be unchanged during propagation. The resulting calculation of the oscillation probabilities is identical in both the simplified version and the full derivation.

To begin, equation 2.7 is expanded by explicitly including the complex conjugate,

$$P\left(\nu_\alpha \to \nu_\beta\right) = \sum_i^3 U_{\beta i}^* U_{\alpha i} \sum_j U_{\beta j} U_{\alpha j}^* e^{i(E_i - E_j)t} \quad \alpha, \beta = e, \mu\tau. \tag{2.8}$$

In the highly relativistic limit, $E \gg m_i$, and $t \approx L$ where L is the distance traveled during propation. Using these two approximations, the exponential term in Equation 2.7 may be rewritten using Euler's formula

$$e^{i(E_i - E_j)t} = 1 - 2\sin^2\left(\frac{m_{ij}^2 L}{4E}\right) + i\sin\left(\frac{m_{ji}^2 L}{2E}\right) \tag{2.9}$$

Note that a new shorthand has been defined, $\Delta m_{ji}^2 = m_j^2 - m_i^2$, giving a fundamental parameter of neutrino oscillations. The PMNS terms of equation 2.8 may be expanded further, yielding

$$\left|\sum_j U_{\beta j} U_{\alpha j}^*\right|^2 = \delta_{\alpha\beta} + 2\sum_{i<j}\sum_i U_{\beta i}^* U_{\alpha i} U_{\beta j} U_{\alpha j}^* \tag{2.10}$$

where the factor of two arises due to the symmetry $i \leftrightarrow j$. Putting the terms together, the final oscillation probability formula is

$$\begin{aligned} P\left(\nu_\alpha \to \nu_\beta\right) = \delta_{\alpha\beta} &- 4\sum_{i<j} Re\left[\sum_i U_{\beta i}^* U_{\alpha i} U_{\beta j} U_{\alpha j}^*\right] sin^2\left(\frac{m_{ij}^2 L}{4E}\right) \\ &+ 2\sum_{i<j} Im\left[\sum_i U_{\beta i}^* U_{\alpha i} U_{\beta j} U_{\alpha j}^*\right] sin\left(\frac{m_{ji}^2 L}{2E}\right). \end{aligned} \tag{2.11}$$

This calculation has been derived for neutrinos. To calculate the probabilities for anti-neutrinos, the calculation changes by replacing $U \to U^*$, resulting in a change in sign of the last term of Equation 2.11.

From Equation 2.11, the general form of the oscillation probabilities becomes clear. The PMNS matrix elements yield the amplitude of oscillations, while the phase of the oscillations is related to three quantities: the squared difference in the masses, Δm_{ji}^2; the baseline, or distance traveled, L; and the energy of the neutrinos. Only one of these three is a fundamental physics parameter. The choices of energy sensitivity and baseline are used to define characteristics of detectors used for measurements of the various mass splitting parameters and oscillation mixing angles.

Note that the oscillation probability is insensitive to the sign of the mass splitting parameter.

2.1.3 Matter Effects in Oscillation

Calculations up to this point have assumed neutrinos oscilating in vacuum. Modifications required for a description of matter effects begin with a modification of the Hamiltonian

with a potential, V, due to coherent forward scattering of neutrino on electrons and nucleons in the medium [43].

$$H = H_0 + V \tag{2.12}$$

The value of H_0 is the value of vacuum Hamiltonian. In the two-flavor case, the Hamiltonian can be shown [40, 44] to be

$$H_0 = \frac{\Delta m^2}{4E}\begin{pmatrix} -2\cos 2\theta & \sin 2\theta \\ \sin 2\theta & 0 \end{pmatrix}. \tag{2.13}$$

where θ is the mixing angle associated with the 2x2 PMNS matrix. If this effect leaves the neutrino momentum unchanged, the resulting additional terms in the Hamiltonian may interfere with the propagation of the unscattered neutrinos. The potential includes contributions from both charged current and neutral current interactions, although the charged current interactions arise solely from the electron neutrinos. The potential, expressed in the flavor basis, is then

$$V_{CC,\alpha} = \begin{cases} \sqrt{2} \pm G_F n_e\left(x\right) & \alpha = e \\ 0 & \alpha = \mu, \tau \end{cases} \qquad V_{NC,\alpha} = -\frac{G_F}{\sqrt{2}} n_e\left(x\right) \quad \alpha = e, \mu, \tau \tag{2.14}$$

where a + is used for neutrinos and a - is used for antineutrinos, n_e is the density of electrons in the medium, and G_F is the Fermi coupling constant. Note that the angle included here is that of the PMNS matrix in two dimensions. A full description of three flavor neutrino oscillation in the presence of a matter potential is beyond the scope of this work. Further information and explicit forms may be found in [40, 44]. The full three-flavor oscillation calculation is used for this thesis using the Prob3++ code [45, 46], which includes an implementation of matter effects. The electron densities are calculated from the Preliminary Reference Earth Model (PREM) [47].

2.2 Experimental Constraints on Neutrino Oscillations

2.3 Solar Neutrinos: A Hint of Multiple Flavors

Early searches for neutrinos focused primarily on the Sun. The first major experiment, proposed by Ray Davis and John Bahcall, was designed to verify that fusion was the primary energy source of the Sun [48, 49]. While the core of the sun is not directly visible to telescopes, neutrinos produced via nuclear fusion could escape the sun relatively unchanged and be observed at Earth.

The Homestake experiment, named for Homestake mine in South Dakota, used 615 tons of perchloroethylene to measure neutrinos via the inverse beta decay reaction

$$\nu_e + {}^{37}Cl \rightarrow {}^{37}Ar + e^- \tag{2.15}$$

The production rate was well-measured, with a rate of 0.48 counts per day and a background of 0.09 counts per day due to interactions from cosmic ray induced muons [50]. In the typical units of the solar neutrino experiments, this worked out to

$$(\sigma\phi) = 2.56 \pm 0.16 \pm 0.16\ SNU \tag{2.16}$$

where 1 SNU $= 10^{-36}$ captures/nucleus/second. The expected rate of neutrino interactions from the sun, however, was prediced to be 8.00 ± 0.97 SNU given the solar models at the time. The Homestake experiment, therefore, was only observing approximately 30% of the prediced interaction rate. New measurements from other experiments, such has SAGE [51], GALLEX [52], and GNO [53] confirmed the results, although with a reduction of around 50% instead of 70% compared to theoretical expectations.

The disagreement between the number of neutrinos expected and the number predicted was not definitively solved until the Sudbury Neutrino Observator (SNO) experiment. SNO was a detector located 2 km underground in Sudbury mine in Canada [34]. The detector consisted of a large tank filled with heavy water surrounded by photo-multiplier tubes for the detection of Cherenkov emission. By introducing heavy water, SNO was sensitive to not only the charged current interactions of previous experiments, but also to neutral current interactions invisible to the inverse beta decay experiments.

SNO detected the neutral current and charged current interactions via two distinct channels. The charged-current interactions caused a deuterium atom to break down into two separate protons while also transforming the neutrino into an electron. The electron would be produced with an energy high enough to emit Cherenkov radiation and could, therefore, be observed directly, with the energy of the electron used to constrain the incident neutrino spectrum. The primary charged current interaction at SNO was only sensitive to electron flavor neutrino interactions.

The neural current interactions, with a threshold energy of 2.22 MeV, were able to separate the deuterium in the heavy water, leading to a free neutron in the detector. The detection of the free neutron posed initial challenges for the same fundamental reason that neutrino detection is difficult: neutrons are not charged and therefore do not emit electromagnetic radiation. Instead, early detections of these neutrons relied on the emission of a high energy gamma ray when the neutron was captured on a deuterium atom. The gamma ray could then, in turn, be absorbed on an electron, accerating the charged particle and producing Cherenkov radiation.

Measurements at SNO were divided between these two measurement channels in order to investigate one possible solution to the missing solar neutrinos: neutrino oscillations [54]. Because the three known neutrino states all have the same neutral current interaction cross section, the neutral current rate is expected to be constant in the presence of oscillations. The charged current rate is, however, expected to change due to the different couplings of each neutrino flavor to the $W^{\pm}$ boson. Measuring both the neutral current and charged current rates therefore provided a direct test of neutrino oscillations, allowing researchers to identify the effect independent of the solar model.

SNO expected a rate of neutral current interactions from solar neutrinos of $5.05 \times 10^6 cm^{-2} s^{-1}$ and observed

$$\phi_{NC}\left(\nu\ active\right) = 5.25 \pm 0.16(stat)^{+0.11}_{-0.13} \times 10^6 cm^{-2} s^{-1} \tag{2.17}$$

a result consistent with expectations. The charged current interaction was measured to be

$$\phi_{CC}\left(\nu_e\right) = \left(0.301 \pm 0.033\right) \phi_{NC}\left(\nu\ active\right) \tag{2.18}$$

clearly indicating that the number of electron neutrinos was well below expectations. The combination of these two results gave the first clear indication of neutrino oscillations, a result which earned the SNO collaboration a Nobel Prize in 2015 [55].

2.4 Super-Kamiokande and Atmospheric Neutrinos

While the SNO experiment awas working to identify the source of the solar neutrino deficit, the Kamioka Nucleon Decay Experiment (KamiokaNDE) and its successor, Super-Kamiokande (Super-K), were using a similar water Cherenkov detector to search for proton decay. The primary background for this rare process is neutrino interactions. Unlike SNO, however, Super-Kamiokande was sensitive to both MeV solar neutrinos and higher energy GeV neutrinos produced in the atmospheric showers from cosmic ray interactions.

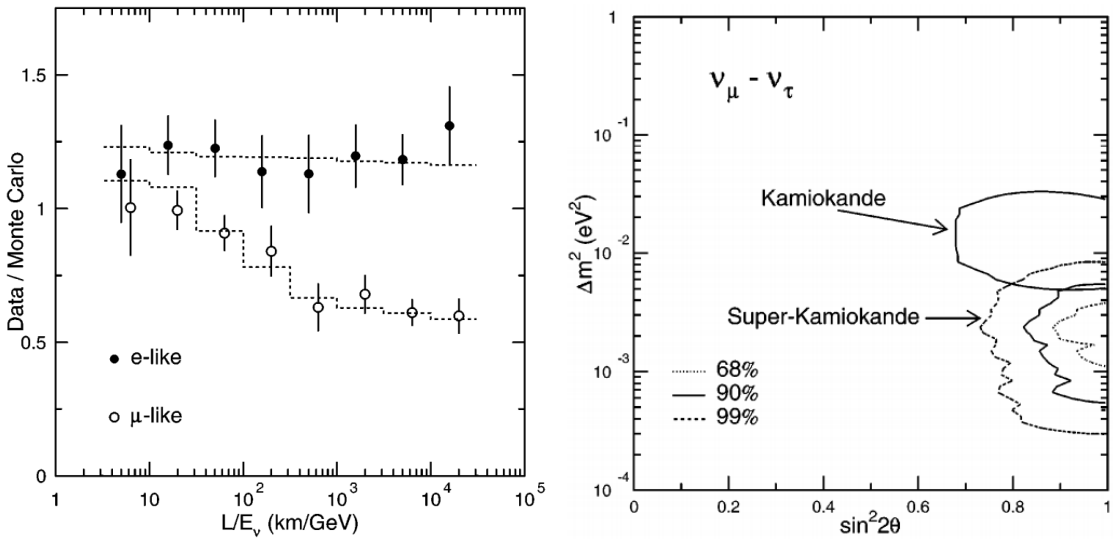

(a) L/E From [56]

(b) Oscillation Measurement from [56]

Figure 2.1 – The first atmospheric neutrino oscillation measurements from the Super-K experiment. (a) The ν_e-like events show no shape in L/E, as expected from a lack of neutrino oscillations. The ν_μ-like interactions, however, show a clear drop, indicating the presence of oscillation effects. (b) Using the two neutrino approximation, Super-K produced contours of the best-fit oscillation parameters for $\nu_\mu \rightarrow \nu_\tau$ oscillations. Both figures from [56]

While investigating backgrounds, Super-Kamiokande observed an interesting deficit in the atmospheric neutrino signal. Unlike the case in the solar neutrinos, the deficit observed by Super-K was observed solely in the muon neutrino events with no effect seem in the electron neutrinos [56]. Using the reconstructed energy and direction of events, Super-K was able to show that the number of fully contained events of ν_μ-like interactions changed as a function of L/E - a clear signature of neutrino oscillations in the atmospheric neutrinos. The figure, reproduced in Figure 2.1a, was used, in part, with an 2x2 approximation to the PMNS matrix to produce the first measurements, shown in Figure 2.1b, of the atmospheric oscillation parameters. For the discovery of atmospheric neutrino oscillations at the same time as SNO's discovery of solar neutrino oscillations, the Super-K collaboration was jointly award the 2015 Nobel Prize [55].

2.4.1 Global Fits to Oscillations

Since the initial discoveries of SNO and Super-K, many experiments have measured neutrino oscillations. Global fits are performed and updated regularly [57, 58].

The most recent results are shown in Figure 2.2 and include information from solar, reactor, and atmospheric oscillation experiments. The results explicitly assume unitarity and three neutrino species.

NuFIT 3.2 (2018)

	Normal Ordering (best fit)		Inverted Ordering ($\Delta\chi^2 = 4.14$)		Any Ordering
	bfp $\pm 1\sigma$	3σ range	bfp $\pm 1\sigma$	3σ range	3σ range
$\sin^2\theta_{12}$	$0.307^{+0.013}_{-0.012}$	$0.272 \to 0.346$	$0.307^{+0.013}_{-0.012}$	$0.272 \to 0.346$	$0.272 \to 0.346$
$\theta_{12}/^\circ$	$33.62^{+0.78}_{-0.76}$	$31.42 \to 36.05$	$33.62^{+0.78}_{-0.76}$	$31.43 \to 36.06$	$31.42 \to 36.05$
$\sin^2\theta_{23}$	$0.538^{+0.033}_{-0.069}$	$0.418 \to 0.613$	$0.554^{+0.023}_{-0.033}$	$0.435 \to 0.616$	$0.418 \to 0.613$
$\theta_{23}/^\circ$	$47.2^{+1.9}_{-3.9}$	$40.3 \to 51.5$	$48.1^{+1.4}_{-1.9}$	$41.3 \to 51.7$	$40.3 \to 51.5$
$\sin^2\theta_{13}$	$0.02206^{+0.00075}_{-0.00075}$	$0.01981 \to 0.02436$	$0.02227^{+0.00074}_{-0.00074}$	$0.02006 \to 0.02452$	$0.01981 \to 0.02436$
$\theta_{13}/^\circ$	$8.54^{+0.15}_{-0.15}$	$8.09 \to 8.98$	$8.58^{+0.14}_{-0.14}$	$8.14 \to 9.01$	$8.09 \to 8.98$
$\delta_{CP}/^\circ$	234^{+43}_{-31}	$144 \to 374$	278^{+26}_{-29}	$192 \to 354$	$144 \to 374$
$\frac{\Delta m^2_{21}}{10^{-5}\ \mathrm{eV}^2}$	$7.40^{+0.21}_{-0.20}$	$6.80 \to 8.02$	$7.40^{+0.21}_{-0.20}$	$6.80 \to 8.02$	$6.80 \to 8.02$
$\frac{\Delta m^2_{3\ell}}{10^{-3}\ \mathrm{eV}^2}$	$+2.494^{+0.033}_{-0.031}$	$+2.399 \to +2.593$	$-2.465^{+0.032}_{-0.031}$	$-2.562 \to -2.369$	$\begin{bmatrix}+2.399 \to +2.593\\ -2.536 \to -2.395\end{bmatrix}$

Figure 2.2 – The global best-fit values for the three flavor neutrino oscillation fits as of November 2017. The first column shows results assuming the normal ordering while the second colum shows the results for the inverted ordering. Image taken from [58]

2.5 Unitarity and Sterile Neutrinos

While global fits assume three flavors of neutrinos, additional neutrino flavors are theoretically possible. The number of active neutrino flavors is limited to the three known flavors from the measurements of ALEPH (see the discussion of Section 1), although such measurements implicitly only measure the number of species with a coupling to the Z boson [9]. Additional flavors with no or very small couplings to the Z boson may be allowed [59]. New neutrino flavors introduced with these properties are known as *sterile neutrinos*.

2.5.1 Sterile Neutrinos

Models of sterile neutrinos assume that no weak interactions are available to the new species, leaving only interactions with the world via oscillations. In this model, neutrinos oscillate using a 4x4 (or larger NxN) PMNS matrix [40, 60, 61, 59].

$$\begin{pmatrix}\nu_e(x)\\ \nu_\mu(x)\\ \nu_\tau(x)\\ \nu_s(x)\end{pmatrix} = U_{4x4}\begin{pmatrix}\nu_e(x)\\ \nu_\mu(x)\\ \nu_\tau(x)\\ \nu_s(x)\end{pmatrix} = \begin{pmatrix}U_{e1} & U_{e2} & U_{e3} & U_{e4}\\ U_{\mu1} & U_{\mu2} & U_{\mu3} & U_{\tau4}\\ U_{\tau1} & U_{\tau2} & U_{\tau3} & U_{\tau4}\\ U_{s1} & U_{s2} & U_{s3} & U_{s4}\end{pmatrix}\begin{pmatrix}\nu_1(x)\\ \nu_2(x)\\ \nu_3(x)\\ \nu_4(x)\end{pmatrix} \tag{2.19}$$

The additional terms in U_{4x4} lead to new mixing angles, θ_{14}, θ_{24}, and θ_{34}. The new terms may be used in the standard oscillation framework introduced in Section 2.1.1 extended with a fourth flavor state, ν_s, and mass state, ν_4.

$$P(\nu_\alpha \to \nu_\beta) = \sum_i^4 U^*_{\beta i}U_{\alpha i}\sum_j U_{\beta j}U^*_{\alpha j}e^{i(E_i-E_j)t} \quad \alpha,\beta = e,\mu\tau,s \tag{2.20}$$

Unlike the three active neutrinos, sterile neutrinos cannot interact with matter, leading to a deficit in the neutrino rates from oscillations of the form $P(\nu_\alpha \to \nu_s)$. The location and size of the deficit is determined by the oscillation parameters associated with the ν_s and ν_4 states. Sterile neutrinos may be indirectly observed through this deficit by studying the active neutrinos with either charged current or neutral current interactions.

2.5.2 Direct Searches for Steriles

While oscillation of the three active neutrinos preserves the total neutral current rate, sterile neutrinos do not. This provide a unique experimental signature for sterile neutrinos. Dedicated searches for this disappearance have been performed by MINOS [62, 63] and NOνA [64] with assumptions on the new terms of the mixing matrix. The effect of three sterile hypotheses on the MINOS data is shown in Figure 2.3a. Around 15% of the neutral current events disappear in the three hypotheses tested by MINOS. The results of the NOνA search are shown in Figure 2.3b.

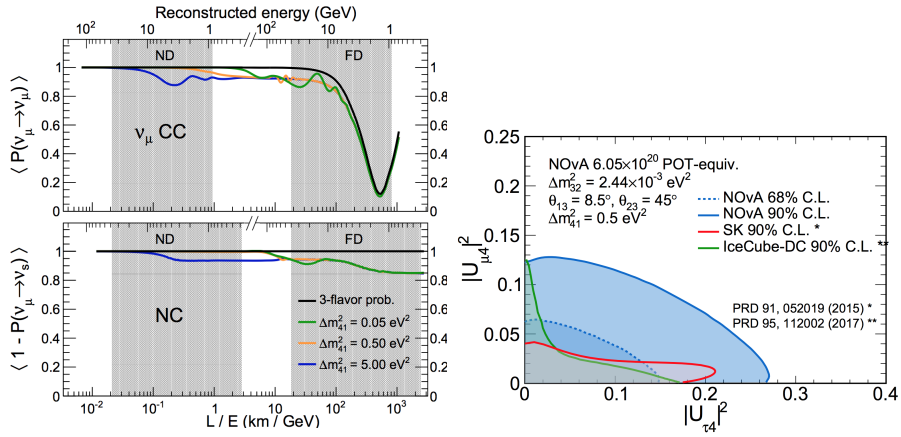

(a) MINOS NC Sterile Expectation **(b)** NOνA Limits from NC Oscillations

Figure 2.3 – Expectations (a) and results (b) of searches for sterile neutrinos in the neutural current interactions. (a) Effect of three hypothetical sterile neutrinos on the measurements of the MINOS detector [63]. "ND" and "FD" refer to the near and far detector of MINOS respectively. The sterile neutrinos have a small effect on the main oscillation minimum in the charged current channel, but up to 15% of the neutral current events are lost. (b) The results of the NOνA search for sterile neutrinos using neutral current events. The limits are interpreted in terms of the 4x4 PMNS mixing elements in order to compare to searches with charged current interactions in Super-Kamiokande [65] and IceCube [66].

Most experiments attempt to investigate one of the additional terms only, assuming the remainder to be negligible [65, 66, 67]. The results rule out large mixing between a hypothetical sterile neutrino and the three active flavors, although small mixing angles are still allowed by experiments [61, 59].

2.5.3 Indirect Searches for Steriles Using Unitarity

Experiments need not search for direct evidence of new mixing terms, however. The addition of a fourth generation of neutrino would have consequences for neutrino oscillation measurements performed in the 3x3 PMNS framework. Standard 3-flavor oscillation measurements may therefore be used to place limits on sterile neutrinos.

The PMNS matrix gives the change in basis and is assumed to be unitary. The unitary condition imposes summation rules for both the rows and colums of the matrix.

$$\sum_i U_{\alpha i} U^*_{\beta i} = \delta_{\alpha\beta} \quad \alpha, \beta = e, \mu, \tau \tag{2.21}$$

$$\sum_i U_{\alpha i} U^*_{\alpha j} = \delta_{ij} \quad i, j = 1, 2, 3 \tag{2.22}$$

If the neutrino mixing matrix consists of more than the three known active neutrinos, however, these unitary relations would only hold in higher dimensions. When projected down to the observed 3x3 PMNS matrix, non-unitarity would be observed.
Neutrino oscillation measurements are performed with the assumption of 3x3 unitarity imposed, allowing the PMNS matrix to be rewritten in terms of three mixing angles and a single phase. The appearance and disappearance probabilities in oscillation measurements are typically written in terms of these mixing angles. Using these mixing angles, the disappearance probability for atmospheric oscillations of $\nu_\mu \to \nu_\tau$ is given by

$$\begin{aligned} P(\nu_\mu \to \nu_\mu) &= 1 - \left| \sum_i U^*_{\mu i} U_{\mu i} e^{-i m_i^2 L/2E} \right|^2 \\ &= 1 - \left(cos^2\theta_{13} sin^2 2\theta_{23} + sin^4\theta_{23} sin^2 2\theta_{13} \right) sin^2 \left(\frac{\Delta m^2_{31} L}{4E} \right) \\ &\approx 1 - sin^2 2\theta_{23} sin^2 \left(\frac{\Delta m^2_{31} L}{4E} \right). \end{aligned} \tag{2.23}$$

where the final approximation has been made due to the small value of θ_{13}. The atmospheric appearance probability, $\nu_\mu \to \nu_\mu$, is given by

$$\begin{aligned} P(\nu_\mu \to \nu_\tau) &= \left| \sum_i U^*_{\mu i} U_{\tau i} e^{-i m_i^2 L/2E} \right|^2 \\ &= \left(cos^2\theta_{13} sin^2 2\theta_{23} + sin^4\theta_{23} sin^2 2\theta_{13} \right) sin^2 \left(\frac{\Delta m^2_{31} L}{4E} \right) \\ &\approx sin^2 2\theta_{23} sin^2 \left(\frac{\Delta m^2_{31} L}{4E} \right). \end{aligned} \tag{2.24}$$

The form of the oscillation probabilities for appearance and disappearance are very similar when written in terms of the mixing angles. However, the appearance and appearance probabilities in neutrino oscillation measurements depend on different elements of PMNS mixing matrix. Because of the difference in the elements probed, appearance and disappearance measurements may be interpreted to give limits on the fundamental elements of the mixing matrix without imposing unitary.
This method of searching for sterile neutrinos may be applied to global fits, reinterpreting standard oscillation measurements to place limits on the size of any non-unitarity. Using the unitarity conditions of Equation 2.21 and 2.22, limits on the size of non-untarity have been calculated[68]. Experimental constraints from a number of experiments (see reference 26 of [68]) were used to evaluate the best-fit mixing matrix. The unitarity constraints were tested by looking at the potential deviation of each row or column

$$\Delta U_\alpha = 1 - \left(|U_{\alpha 1}|^2 + |U_{\alpha 2}|^2 + |U_{\alpha 3}|^2 \right) \quad \alpha = e, \mu, \tau \tag{2.25}$$

or

$$\Delta U_i = 1 - \left(|U_{\alpha i}|^2 + |U_{\beta i}|^2 + |U_{\delta i}|^2\right) \quad i = 1, 2, 3 \tag{2.26}$$

The results are shown in 2.4. The contraints on unitarity of the 3x3 mixing matrix are strongest in the muon and electron sector, with constraints nearly an order of magnitude stronger than that observed in the tau sector. This is a result of limited measurements directly involving ν_τ oscillations.

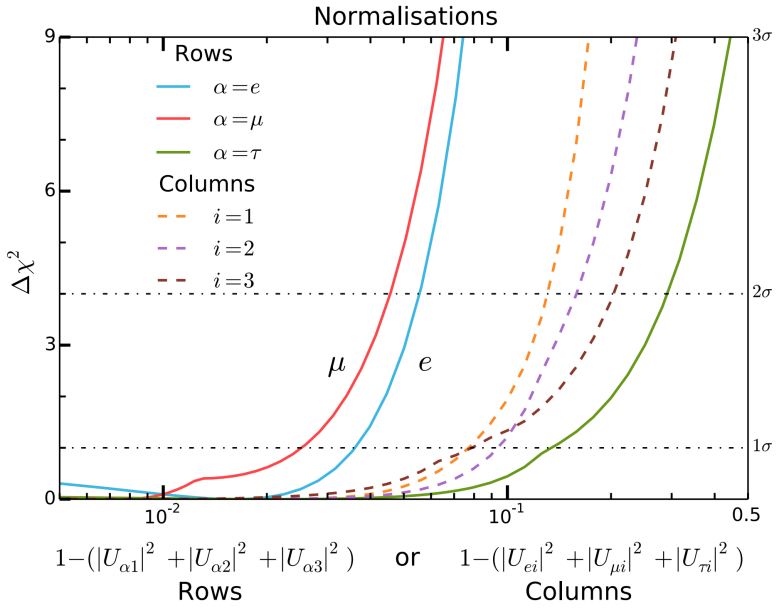

Figure 2.4 – The results of the tests using 2.25 (solid) and 2.26 (dotted). A smaller value on the x-axis indicates a tighter constraint on observed unitarity of the 3x3 mixing matrix. Tests involving only muon or electron flavors show significantly tighter constraints than those including the tau flavor. Image taken from [68]

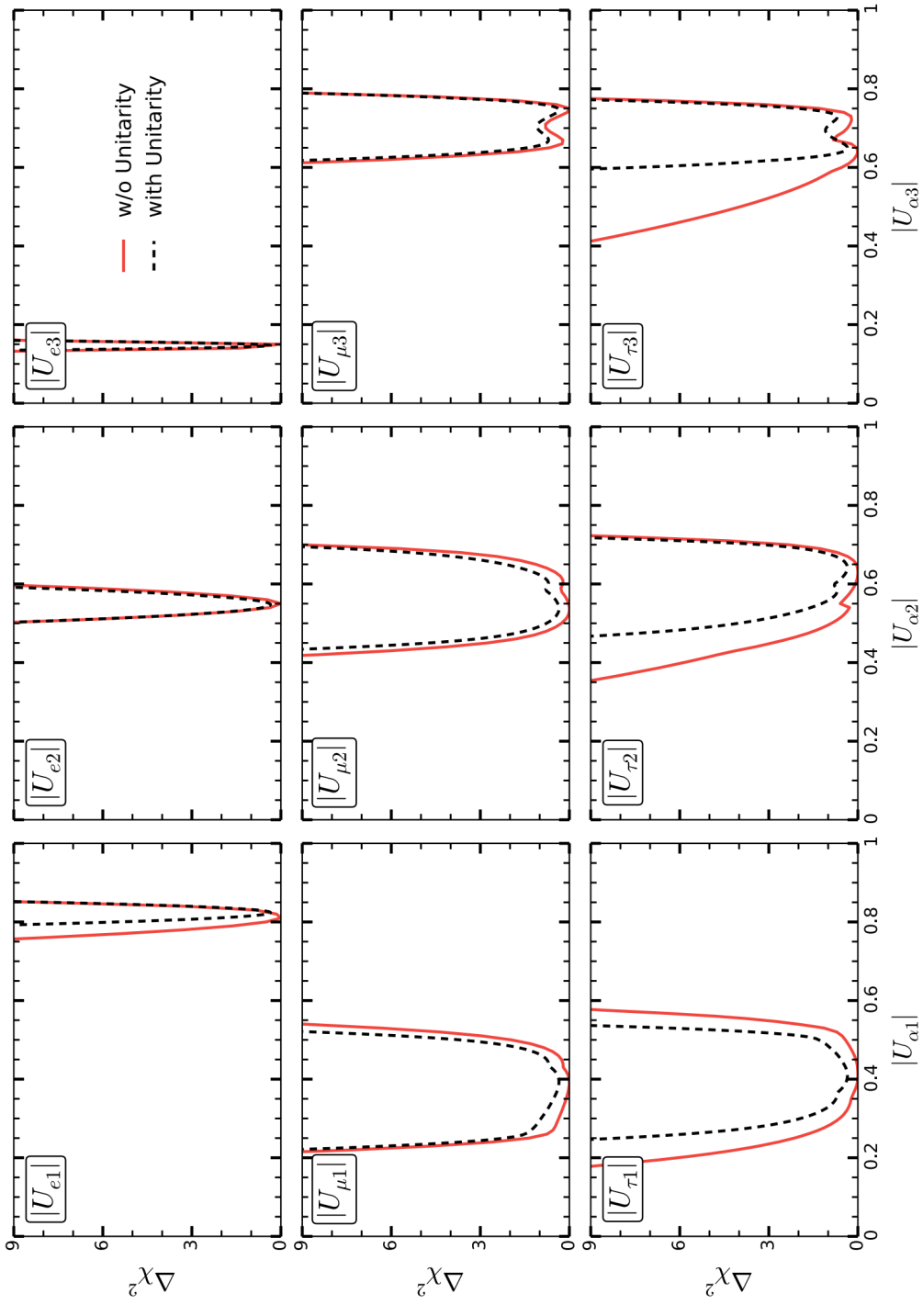

Figure 2.5 – The constraints from a global fit to neutrino oscillation data[68] with an assumption of unitarity (black dotted) or no assumption of unitarity (red solid). The first two rows show little change from the unitarity assumption, indicating strong constraints from direct measurements. The elements of the third row, related to the ν_τ, show much larger changes, indicating that constraints are obtained from indirect oscillation measurements.

When the individual limits for each element of the 3x3 PMNS matrix are checked, it is the tau sector that shows the largest uncertainties. Measurements of ν_τ oscillations therefore can provide valuable information on unitarity in the neutrino sector, leading to indirect constaints on sterile neutrino hypotheses.

Bibliography

[1] H. Becquerel. "Sur les radiations émises par phosphorescence". In: *Comptes Rendus* 122 (1896) (cit. on p. 8).

[2] J Chadwick. "Intensitatsverteilung im magnetischen Spectrum der β-Strahlen von radium B + C". In: *Verhandl. Dtsc. Phys. Ges.* 16 (1914), p. 383 (cit. on p. 8).

[3] W. Pauli. *Offener Brief an die Gruppe der Radioaktiven bei der Gauvereins-Tagung zu Tübingen*. ETH Zürich, 1930 (cit. on p. 8).

[4] C. L. Cowan Jr., F. Reines, F. B. Harrison, H. W. Kruse, and A. D. McGuire. "Detection of the Free Neutrino: A Confirmation". In: *Science* 124 (July 1956), pp. 103–104 (cit. on p. 8).

[5] Nobel Foundation. *Nobel Prize in Physics*. 1995 (cit. on p. 9).

[6] G. Danby, J-M. Gaillard, K. Goulianos, et al. "Observation of High-Energy Neutrino Reactions and the Existence of Two Kinds of Neutrinos". In: *Phys. Rev. Lett.* 9 (1 1962), pp. 36–44 (cit. on p. 9).

[7] DONUT Collaboration, K. Kodama, N. Ushida, et al. "Observation of tau neutrino interactions". In: *Physics Letters B* 504 (Apr. 2001), pp. 218–224. eprint: `hep-ex/0012035` (cit. on pp. 9, 16).

[8] K. Kodama, N. Ushida, C. Andreopoulos, et al. "Final tau-neutrino results from the DONuT experiment". In: *Phys. Rev. D* 78.5, 052002 (Sept. 2008), p. 052002. arXiv: `0711.0728 [hep-ex]` (cit. on p. 9).

[9] The ALEPH Collaboration, the DELPHI Collaboration, the L3 Collaboration, et al. "Precision Electroweak Measurements on the Z Resonance". In: *ArXiv High Energy Physics - Experiment e-prints* (Sept. 2005). eprint: `hep-ex/0509008` (cit. on pp. 9, 25).

[10] A. De Angelis. "Domenico Pacini, uncredited pioneer of the discovery of cosmic rays". In: *ArXiv e-prints* (Mar. 2011). arXiv: `1103.4392` (cit. on p. 10).

[11] J. R. Hoerandel. "Early cosmic-ray work published in German". In: *American Institute of Physics Conference Series*. Ed. by J. F. Ormes. Vol. 1516. American Institute of Physics Conference Series. Feb. 2013, pp. 52–60. arXiv: `1212.0706` (cit. on p. 10).

[12] Arthur H. Compton. "A Geographic Study of Cosmic Rays". In: *Phys. Rev.* 43 (6 1933), pp. 387–403 (cit. on p. 10).

[13] Nobel Foundation. *Nobel Prize in Physics*. 1936 (cit. on p. 10).

[14] M Blau and H Wambacher. "Disintegration Processes by Cosmic Rays with the Simultaneous Emission of Several Heavy Particles". In: 140 (Jan. 1937), pp. 585–585 (cit. on p. 10).

[15] W. Bothe and W. Kolhoerster. "Das Wesen der Hoehenstrahlung". In: *Zeitschrift fur Physik* 56 (Nov. 1929), pp. 751–777 (cit. on p. 10).

[16] G. W. Clark, J. Earl, W. L. Kraushaar, et al. "Cosmic-Ray Air Showers at Sea Level". In: *Phys. Rev.* 122 (2 1961), pp. 637–654 (cit. on p. 10).

[17] K. A. Olive et al. "Review of Particle Physics". In: *Chin. Phys.* C38 (2014), p. 090001 (cit. on pp. 10, 11, 16, 17, 21).

[18] M. Honda, M. S. Athar, T. Kajita, K. Kasahara, and S. Midorikawa. "Atmospheric neutrino flux calculation using the NRLMSISE-00 atmospheric model". In: *Phys. Rev. D* 92.2, 023004 (July 2015), p. 023004. arXiv: `1502.03916 [astro-ph.HE]` (cit. on pp. 10, 12).

[19] Wikimedia Commons. *File:Standard Model of Elementary Particles.svg — Wikimedia Commons, the free media repository.* [Online; accessed 23-February-2018]. 2017 (cit. on p. 13).

[20] J. A. Formaggio and G. P. Zeller. "From eV to EeV: Neutrino cross sections across energy scales". In: *Reviews of Modern Physics* 84 (July 2012), pp. 1307–1341. arXiv: `1305.7513 [hep-ex]` (cit. on pp. 14, 15).

[21] D. Chirkin and W. Rhode. "Propagating leptons through matter with Muon Monte Carlo (MMC)". In: *ArXiv High Energy Physics - Phenomenology e-prints* (July 2004). eprint: `hep-ph/0407075` (cit. on p. 16).

[22] H. Pessard. "The Opera Experiment". In: *High Energy Physics, ICHEP 2004*. Ed. by H. Chen, D. Du, W. Li, and C. Lu. Apr. 2005, pp. 299–303. eprint: `hep-ex/0504033` (cit. on p. 16).

[23] Minos Collaboration, D. G. Michael, P. Adamson, et al. "The magnetized steel and scintillator calorimeters of the MINOS experiment". In: *Nuclear Instruments and Methods in Physics Research A* 596 (Nov. 2008), pp. 190–228. arXiv: `0805.3170 [physics.ins-det]` (cit. on p. 16).

[24] S. Mufson, B. Baugh, C. Bower, et al. "Liquid scintillator production for the NOvA experiment". In: *Nuclear Instruments and Methods in Physics Research A* 799 (Nov. 2015), pp. 1–9. arXiv: `1504.04035 [physics.ins-det]` (cit. on p. 16).

[25] L. Aliaga and et al. "Design, calibration, and performance of the MINERvA detector". In: *Nuclear Instruments and Methods in Physics Research A* 743 (Apr. 2014), pp. 130–159. arXiv: `1305.5199 [physics.ins-det]` (cit. on p. 16).

[26] Y. Kudenko and T2K Collaboration. "The near neutrino detector for the T2K experiment". In: *Nuclear Instruments and Methods in Physics Research A* 598 (Jan. 2009), pp. 289–295. arXiv: `0805.0411 [physics.ins-det]` (cit. on p. 16).

[27] M. Antonello, B. Baibussinov, V. Bellini, et al. "ICARUS at FNAL". In: *ArXiv e-prints* (Dec. 2013). arXiv: `1312.7252 [physics.ins-det]` (cit. on p. 16).

[28] P. A. Čerenkov. "Visible Radiation Produced by Electrons Moving in a Medium with Velocities Exceeding that of Light". In: *Physical Review* 52 (Aug. 1937), pp. 378–379 (cit. on p. 17).

[29] P. A. Cherenkov. "Visible luminescence of pure liquids under the influence of -radiation". In: *Dokl. Akad. Nauk SSSR* 2.8 (1934). [Usp. Fiz. Nauk93,no.2,385(1967)], pp. 451–454 (cit. on p. 17).

[30] I. M. Frank and I. E. Tamm. "Coherent visible radiation of fast electrons passing through matter". In: *Compt. Rend. Acad. Sci. URSS* 14.3 (1937). [Usp. Fiz. Nauk93,no.2,388(1967)], pp. 109–114 (cit. on pp. 17, 18).

[31] D.J. Griffiths. *Introduction to Electrodynamics*. Ed. by Pearson Education Limited. Fourth. 2013 (cit. on p. 17).

[32] S. Tavernier. *Experimental Techniques in Nuclear and Particle Physics*. Ed. by Springer-Verlag. 2010 (cit. on pp. 17, 18).

[33] K.A. Olive and Particle Data Group. "Review of Particle Physics". In: *Chinese Physics C* 38.9 (2014), p. 090001 (cit. on p. 18).

[34] B. Aharmim, S. N. Ahmed, A. E. Anthony, et al. "Combined analysis of all three phases of solar neutrino data from the Sudbury Neutrino Observatory". In: *Phys. Rev. C* 88.2, 025501 (Aug. 2013), p. 025501. arXiv: `1109.0763 [nucl-ex]` (cit. on pp. 18, 23).

[35] C. W. Walter. "The Super-Kamiokande Experiment". In: *Neutrino Oscillations: Present Status and Future Plans*. Ed. by J. A. Thomas and P. L. Vahle. World Scientific Publishing Co, 2008, pp. 19–43 (cit. on p. 18).

[36] F. Montanet. "Design and expected performance of the ANTARES neutrino telescope". In: *Nuclear Physics B Proceedings Supplements* 87 (June 2000), pp. 436–438. eprint: `astro-ph/0001380` (cit. on p. 18).

[37] M. G. Aartsen, M. Ackermann, J. Adams, et al. "The IceCube Neutrino Observatory: instrumentation and online systems". In: *Journal of Instrumentation* 12 (Mar. 2017), P03012. arXiv: `1612.05093 [astro-ph.IM]` (cit. on p. 18).

[38] B. Pontecorvo. "Neutrino Experiments and the Problem of Conservation of Leptonic Charge". In: *Sov. Phys. JETP* 26 (1968). [Zh. Eksp. Teor. Fiz.53,1717(1967)], pp. 984–988 (cit. on p. 19).

[39] Z. Maki, M. Nakagawa, and S. Sakata. "Remarks on the Unified Model of Elementary Particles". In: *Progress of Theoretical Physics* 28 (Nov. 1962), pp. 870–880 (cit. on p. 19).

[40] C. Giganti, S. Lavignac, and M. Zito. "Neutrino oscillations: The rise of the PMNS paradigm". In: *Progress in Particle and Nuclear Physics* 98 (Jan. 2018), pp. 1–54. arXiv: `1710.00715 [hep-ex]` (cit. on pp. 20, 22, 25).

[41] S. T. Petcov. "The Nature of Massive Neutrinos". In: *Adv. High Energy Phys.* 2013 (2013), p. 852987. arXiv: `1303.5819 [hep-ph]` (cit. on p. 20).

[42] E. K. Akhmedov and A. Y. Smirnov. "Paradoxes of neutrino oscillations". In: *Physics of Atomic Nuclei* 72 (Aug. 2009), pp. 1363–1381. arXiv: `0905.1903 [hep-ph]` (cit. on p. 20).

[43] A. Y. Smirnov. "The MSW Effect and Matter Effects in Neutrino Oscillations". In: *Physica Scripta Volume T* 121 (Jan. 2005), pp. 57–64. eprint: `hep-ph/0412391` (cit. on p. 22).

[44] S. M. Bilenky. "Neutrino oscillations: brief history and present status". In: *ArXiv e-prints* (Aug. 2014). arXiv: `1408.2864 [hep-ph]` (cit. on p. 22).

[45] V. Barger, K. Whisnant, S. Pakvasa, and R. J. N. Phillips. "Matter effects on three-neutrino oscillations". In: *Phys. Rev. D* 22 (11 1980), pp. 2718–2726 (cit. on p. 22).

[46] Super-Kamiokande Collaboration. *Prob3++*. 2012 (cit. on p. 22).

[47] Adam M. Dziewonski and Don L. Anderson. "Preliminary reference Earth model". In: *Physics of the Earth and Planetary Interiors* 25.4 (1981), pp. 297 –356 (cit. on p. 22).

[48] John N. Bahcall. "Solar Neutrinos. I. Theoretical". In: *Phys. Rev. Lett.* 12 (11 1964), pp. 300–302 (cit. on p. 22).

[49] Raymond Davis. "Solar Neutrinos. II. Experimental". In: *Phys. Rev. Lett.* 12 (11 1964), pp. 303–305 (cit. on p. 22).

[50] Bruce T. Cleveland, Timothy Daily, Jr. Raymond Davis, et al. "Measurement of the Solar Electron Neutrino Flux with the Homestake Chlorine Detector". In: *The Astrophysical Journal* 496.1 (1998), p. 505 (cit. on p. 22).

[51] J. N. Abdurashitov, V. N. Gavrin, V. V. Gorbachev, et al. "Measurement of the solar neutrino capture rate with gallium metal. III. Results for the 2002-2007 data-taking period". In: *Phys. Rev. C* 80.1, 015807 (July 2009), p. 015807. arXiv: `0901.2200 [nucl-ex]` (cit. on p. 23).

[52] W. Hampel, J. Handt, G. Heusser, et al. "GALLEX solar neutrino observations: results for GALLEX IV". In: *Physics Letters B* 447.1 (1999), pp. 127 –133 (cit. on p. 23).

[53] M. Altmann, M. Balata, P. Belli, et al. "Complete results for five years of GNO solar neutrino observations". In: *Physics Letters B* 616.3 (2005), pp. 174 –190 (cit. on p. 23).

[54] Herbert H. Chen. "Direct Approach to Resolve the Solar-Neutrino Problem". In: *Phys. Rev. Lett.* 55 (14 1985), pp. 1534–1536 (cit. on p. 23).

[55] Nobel Foundation. *Nobel Prize in Physics*. 2015 (cit. on pp. 23, 24).

[56] Y. Fukuda, T. Hayakawa, E. Ichihara, et al. "Evidence for Oscillation of Atmospheric Neutrinos". In: *Phys. Rev. Lett.* 81 (8 1998), pp. 1562–1567 (cit. on p. 24).

[57] J. Bergström, M. C. Gonzalez-Garcia, M. Maltoni, and T. Schwetz. "Bayesian global analysis of neutrino oscillation data". In: *Journal of High Energy Physics* 9, 200 (Sept. 2015), p. 200. arXiv: `1507.04366 [hep-ph]` (cit. on p. 24).

[58] I. Esteban, M. C. Gonzalez-Garcia, M. Maltoni, I. Martinez-Soler, and T. Schwetz (cit. on pp. 24, 25).

[59] S. Gariazzo, C. Giunti, M. Laveder, Y. F. Li, and E. M. Zavanin. "Light sterile neutrinos". In: *Journal of Physics G Nuclear Physics* 43.3, 033001 (Mar. 2015), p. 033001. arXiv: `1507.08204 [hep-ph]` (cit. on pp. 25, 26).

[60] J. M. Conrad, C. M. Ignarra, G. Karagiorgi, M. H. Shaevitz, and J. Spitz. "Sterile Neutrino Fits to Short Baseline Neutrino Oscillation Measurements". In: *ArXiv e-prints* (July 2012). arXiv: `1207.4765 [hep-ex]` (cit. on p. 25).

[61] S. Gariazzo, C. Giunti, M. Laveder, and Y. F. Li. "Updated global 3+1 analysis of short-baseline neutrino oscillations". In: *Journal of High Energy Physics* 6, 135 (June 2017), p. 135. arXiv: `1703.00860 [hep-ph]` (cit. on pp. 25, 26).

[62] P. Adamson, D. J. Auty, D. S. Ayres, et al. "Active to Sterile Neutrino Mixing Limits from Neutral-Current Interactions in MINOS". In: *Physical Review Letters* 107.1, 011802 (July 2011), p. 011802. arXiv: `1104.3922 [hep-ex]` (cit. on p. 26).

[63] P. Adamson, I. Anghel, A. Aurisano, et al. "Search for Sterile Neutrinos Mixing with Muon Neutrinos in MINOS". In: *Physical Review Letters* 117.15, 151803 (Oct. 2016), p. 151803. arXiv: 1607.01176 [hep-ex] (cit. on p. 26).

[64] P. Adamson, L. Aliaga, D. Ambrose, et al. "Search for active-sterile neutrino mixing using neutral-current interactions in NOvA". In: *Phys. Rev. D* 96.7, 072006 (Oct. 2017), p. 072006. arXiv: 1706.04592 [hep-ex] (cit. on p. 26).

[65] K. Abe, Y. Haga, Y. Hayato, et al. "Limits on sterile neutrino mixing using atmospheric neutrinos in Super-Kamiokande". In: *Phys. Rev. D* 91 (5 2015), p. 052019 (cit. on p. 26).

[66] IceCube Collaboration, M. G. Aartsen, M. Ackermann, et al. "Search for sterile neutrino mixing using three years of IceCube DeepCore data". In: *ArXiv e-prints* (Feb. 2017). arXiv: 1702.05160 [hep-ex] (cit. on p. 26).

[67] M. G. Aartsen, K. Abraham, M. Ackermann, et al. "Searches for Sterile Neutrinos with the IceCube Detector". In: *Physical Review Letters* 117.7, 071801 (Aug. 2016), p. 071801. arXiv: 1605.01990 [hep-ex] (cit. on p. 26).

[68] Stephen Parke and Mark Ross-Lonergan. "Unitarity and the three flavor neutrino mixing matrix". In: *Phys. Rev. D* 93 (11 2016), p. 113009 (cit. on pp. 27–29).

Notes